Variant Selection in Grain Boundary Nucleation of Upper Bainite

T. FURUHARA, H. KAWATA, S. MORITO, G. MIYAMOTO, and T. MAKI

The crystallography of bainitic ferrite nucleated at austenite grain boundaries was studied in an Fe-9Ni-0.15C (mass pct) alloy. The relationship between bainitic ferrite orientations (variants) and grain boundary characters, *i.e.*, misorientation and boundary orientation, was examined by electron backscatter diffraction analysis in scanning electron microscopy and serial sectioning observation. Bainitic ferrite holds nearly the Kurdjumov–Sachs (K-S) orientation relationship with respect to the austenite grain into which it grows. At the beginning of transformation, the variants of bainitic ferrite are severely restricted by the following two rules, both advantageous in terms of interfacial energy: (1) smaller misorientation from the K-S relationship with respect to the opposite austenite grain and (2) elimination of the larger grain boundary area by the nucleation of bainitic ferrite. As the transformation proceeds, variant selection establishing plastic accommodation of transformation strain to a larger extent becomes important. Those kinds of variant selection result in formation of coarse blocks for small undercooling.

I. INTRODUCTION

BAINITE has become more important in recent steel technology, because it is dominant in the microstructure of high-strength structural steels for ship building or for line pipe with good welding performance, high-strength and high-ductility steels for automobile parts, and so on. An upper bainite structure, which forms with lath-shaped bainitic ferrite[1] at temperatures typically above 623 K, consists of the substructures similar to lath martensite.[2] A prior austenite grain is divided into packets, each of which consists of a group of laths with the same parallel close-packed plane relationship in the Kurdjumov–Sachs (K-S) orientation relationship. In general, a bainite packet is partitioned into several blocks, each of which contains laths of a single variant of the K-S relationship.

The packet or block size is important in lath martensite for both strengthening[3–5] and toughening.[3,6,7] Recently, the substructure of lath martensite was studied in detail by local orientation measurement with electron backscatter diffraction in scanning electron microscopy (SEM-EBSD).[8–10] It was confirmed that blocks and packets are refined with an increase of carbon content,[9] as previously reported by one of the present authors.[11] More interestingly, preferential formation of specific variant pairs that are misoriented by a relatively low angle (approximately, 10 deg) in a packet was revealed for low carbon alloys,[9] as also confirmed recently in an Fe-Ni alloy.[10]

Application of SEM-EBSD was extended to study the crystallography of bainite structures,[8,12,13] although details of the bainite block/packet structures were not discussed. Variations of the block/packet sizes with transformation temperature, carbon content,[2] and ausforming[14] were first examined systematically by the present authors. At a higher transformation temperature or carbon content, where a driving force of transformation is small, the formation of specific variants of bainitic ferrite is enhanced, resulting in a coarse block size.[2] It was suggested that variants of bainitic ferrite are restricted by the nature of austenite grain boundary, because bainitic ferrite starts to form at austenite grain boundaries. Although such variant selection is often observed during diffusional transformation,[15] there is no study made in martensite/bainite transformations. Thus, the present study aims to clarify the relationship between the variants of bainitic ferrite and the austenite grain boundary, where bainitic ferrite forms by means of SEM-EBSD analysis.

II. MICROSTRUCTURE ANALYSES

A. *Experimental Procedure*

The alloy used is an Fe-9Ni-0.15C (mass pct) ternary alloy. Specimens were austenitized at 1423 K, transformed at 723 K for various periods, and water quenched. This transformation temperature was chosen because coarse blocks were typically observed for the upper bainite structure in the previous study.[2] Microstructures

---

T. FURUHARA, Professor, and G. MIYAMOTO, Assistant Professor, are with the Institute for Materials Research, Tohoku University, Sendai 980-8577, Japan. Contact e-mail: furuhara@imr.tohoku.ac.jp H. KAWATA, formerly Graduate Student, Department of Materials Science and Technology, Kyoto University, Sakyo-ku, Kyoto, 606-8501, Japan, is Researcher, Steel Research Laboratories, Nippon Steel Corporation, Futtsu 293-8511, Japan. S. MORITO, Associate Professor, is with the Department of Materials Science, Shimane University, Matsue, 690-8504, Japan. T. MAKI, Professor Emeritus, Department of Materials Science and Technology, Kyoto University, Sakyo-ku, Kyoto, 606-8501, Japan, is Executive Advisor, Steel Research Laboratories, Nippon Steel Corporation.

were observed by optical microscopy (OM) and scanning electron microscopy (SEM). Orientations of bainitic ferrite (BF) and lath martensite (LM) were measured using a JEOL* JSM-6500F equipped with a EDAX/TSL

---

*JEOL is a trademark of Japan Electron Optics Ltd., Tokyo.

---

orientation imaging microscopy (OIM) system (Mahwah, NJ). The misorientation across a γ grain boundary was estimated from the variant map constructed from the bainitic ferrite and lath martensite. The grain boundary plane of γ was determined by a trace analysis combined with serial sectioning SEM observation.

The untransformed γ matrix at 723 K is transformed to martensite during quenching after the upper bainite transformation in this alloy. Therefore, it is not possible to measure the orientation relationship between BFs and γ directly. However, it is known that LM as well as BF holds nearly the K-S relationship with respect to its γ matrix. Figures 1(a) and (b) show an example of $\langle 001 \rangle_{bcc}$ pole figure for the BFs formed within a single γ grain and the ideal orientation distribution for all the 24 variants of the K-S orientation relationship listed in Table I, respectively. By making a comparison between Figures 1(a) and (b), it is clear that there is good matching between the two plots in small deviation within 5 deg. This characteristic is commonly observed for LM.[9] Thus, it
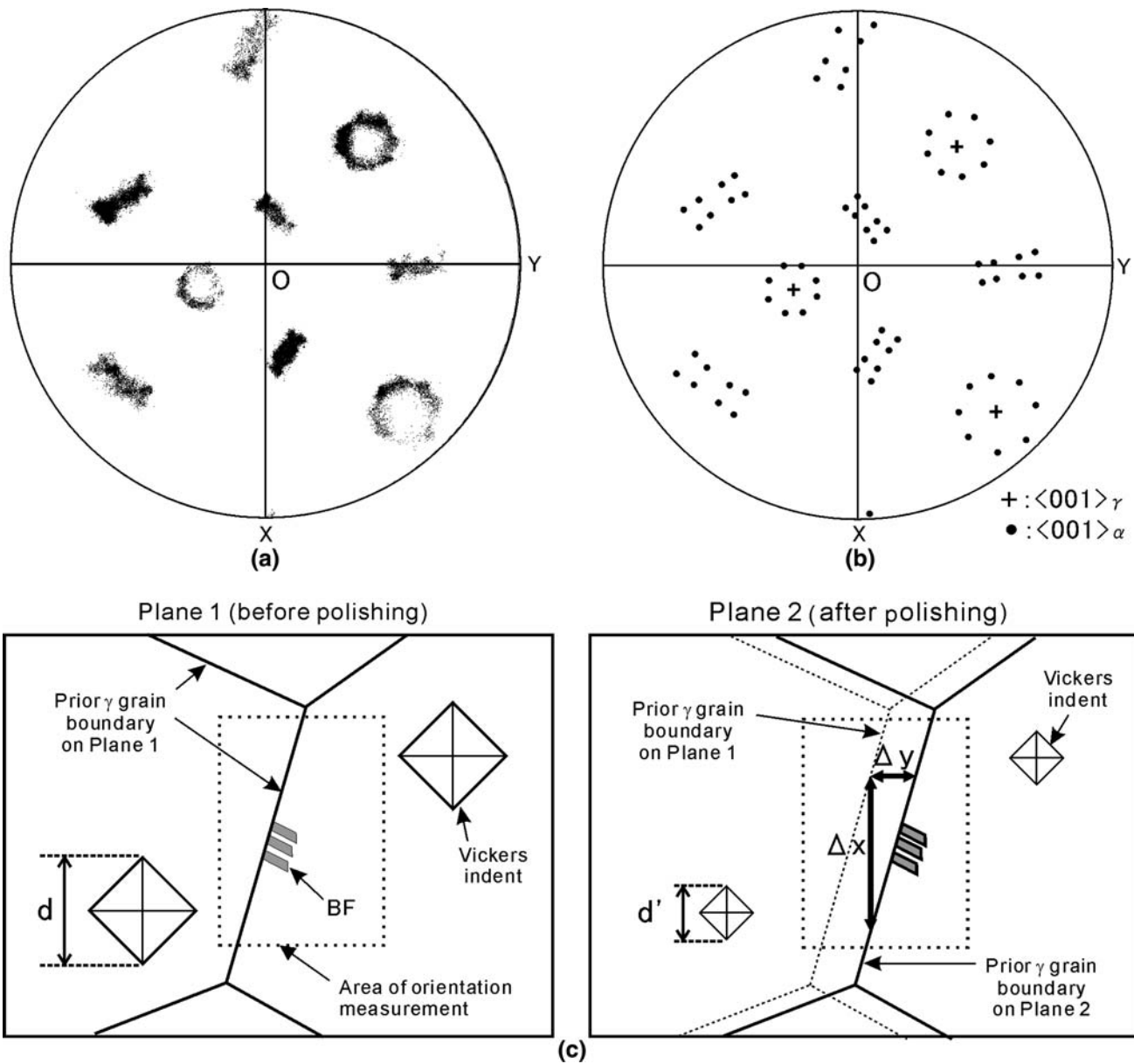

Fig. 1—(a) A typical $\langle 001 \rangle_{bcc}$ pole figure of BFs formed within a single austenite grain (O is the normal direction of the specimen surface observed, and X and Y are the two orthogonal directions on the surface). (b) The corresponding K-S variant map on which $\langle 001 \rangle_{\alpha}$ and $\langle 001 \rangle_{\gamma}$ poles are plotted. (c) Schematic illustrations describing the method of γ grain boundary analysis.

Table I. Intervariant Relationships for the K-S Orientation Relationship

Variant Number	Parallel Plane	Parallel Direction	Rotation from Variant 1
1	$(111)_\gamma//(011)_\alpha$	$[\bar{1}01]_\gamma//[\bar{1}\bar{1}1]_\alpha$	—
2		$[\bar{1}01]_\gamma//[\bar{1}\bar{1}1]_\alpha$	[0.58 −0.58 0.58]/60.0 deg
3		$[01\bar{1}]_\gamma//[\bar{1}\bar{1}1]_\alpha$	[0.00 −0.71 −0.71]/60.0 deg
4		$[01\bar{1}]_\gamma//[\bar{1}\bar{1}1]_\alpha$	[0.00 0.71 0.71]/10.5 deg
5		$[1\bar{1}0]_\gamma//[\bar{1}\bar{1}1]_\alpha$	[0.58 0.71 0.71]/60.0 deg
6		$[1\bar{1}0]_\gamma//[\bar{1}\bar{1}1]_\alpha$	[0.00 −0.71 −0.71]/49.5 deg
7	$(1\bar{1}1)_\gamma//(011)_\alpha$	$[101]_\gamma//[\bar{1}\bar{1}1]_\alpha$	[−0.58 −0.58 0.58]/49.5 deg
8		$[101]_\gamma//[\bar{1}\bar{1}1]_\alpha$	[0.58 −0.58 0.58]/10.5 deg
9		$[\bar{1}\bar{1}0]_\gamma//[\bar{1}\bar{1}1]_\alpha$	[−0.19 0.77 0.61]/50.5 deg
10		$[\bar{1}\bar{1}0]_\gamma//[\bar{1}\bar{1}1]_\alpha$	[−0.49 −0.46 0.74]/50.5 deg
11		$[011]_\gamma//[\bar{1}\bar{1}1]_\alpha$	[0.35 −0.93 −0.07]/14.9 deg
12		$[011]_\gamma//[\bar{1}\bar{1}1]_\alpha$	[0.36 −0.71 0.60]/57.2 deg
13	$(\bar{1}11)_\gamma//(011)_\alpha$	$[0\bar{1}1]_\gamma//[\bar{1}\bar{1}1]_\alpha$	[0.93 0.35 0.07]/14.9 deg
14		$[0\bar{1}1]_\gamma//[\bar{1}\bar{1}1]_\alpha$	[0.74 0.46 −0.49]/50.5 deg
15		$[\bar{1}0\bar{1}]_\gamma//[\bar{1}\bar{1}1]_\alpha$	[−0.25 −0.63 −0.74]/57.2 deg
16		$[\bar{1}0\bar{1}]_\gamma//[\bar{1}\bar{1}1]_\alpha$	[0.66 0.66 0.36]/20.6 deg
17		$[110]_\gamma//[\bar{1}\bar{1}1]_\alpha$	[−0.66 0.36 −0.66]/51.7 deg
18		$[110]_\gamma//[\bar{1}\bar{1}1]_\alpha$	[−0.30 −0.63 −0.72]/47.1 deg
19	$(11\bar{1})_\gamma//(011)_\alpha$	$[\bar{1}10]_\gamma//[\bar{1}\bar{1}1]_\alpha$	[−0.61 0.19 −0.77]/50.5 deg
20		$[\bar{1}10]_\gamma//[\bar{1}\bar{1}1]_\alpha$	[−0.36 −0.60 −0.71]/57.2 deg
21		$[0\bar{1}\bar{1}]_\gamma//[\bar{1}\bar{1}1]_\alpha$	[0.96 0.00 −0.30]/20.6 deg
22		$[0\bar{1}\bar{1}]_\gamma//[\bar{1}\bar{1}1]_\alpha$	[−0.72 0.30 −0.63]/47.1 deg
23		$[101]_\gamma//[\bar{1}\bar{1}1]_\alpha$	[−0.74 −0.25 0.63]/57.2 deg
24		$[101]_\gamma//[\bar{1}\bar{1}1]_\alpha$	[0.91 −0.41 0.00]/21.1 deg
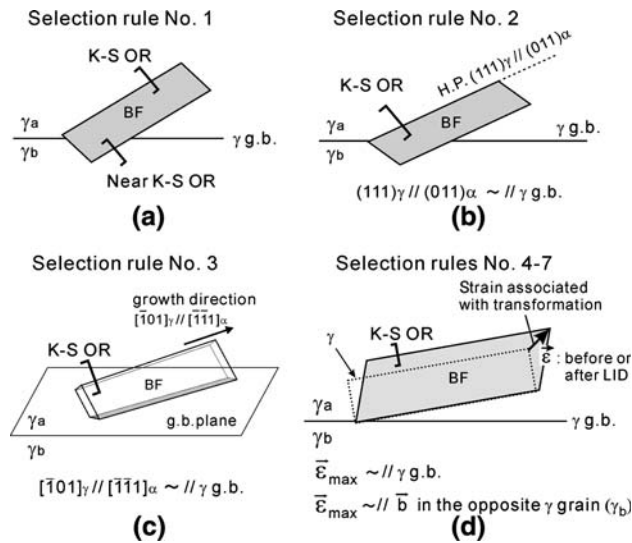
Fig. 2—Schematic illustrations describing various selection rules of BF variants at a γ grain boundary.

can be said that BFs satisfy near the K-S orientation relationship as well as LM. Once the plot such as Figure 1(a) is obtained, the cube axes of the γ matrix can be specified in the plot, as described by the symbol " + " in Figure 1(b). Deriving the rotation matrices accomplishing the orientations of two γ grains forming a grain boundary in the stereographic projection, a misorientation across the grain boundary can be calculated. When the measurements were made for LMs and BFs on both sides of an annealing twin, the measured misorientation of γ grains only deviates by about 1 deg from a Σ3 coincidence site lattice relationship. Thus, this analysis

Fig. 3—Optical micrographs of upper bainite structures in Fe-9Ni-0.15C (B: bainite, and M: martensite): transformed at 723 K for (a) 0.4 ks and (b) for 0.7 ks.

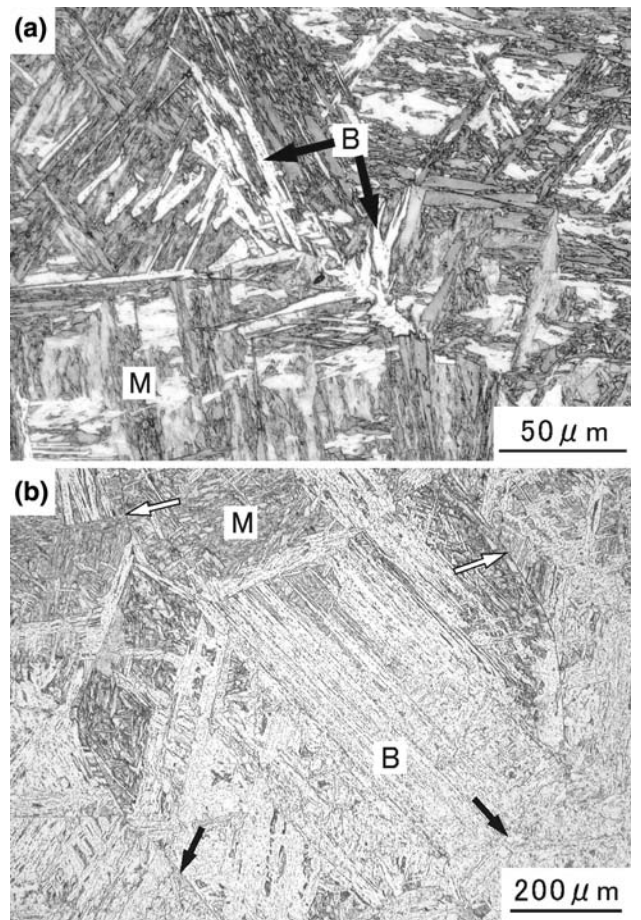**Table II. Characteristics of γ Grain Boundaries with Nucleation of BF in the Fe-9Ni-0.15C Alloy Transformed at 723 K for 0.4 ks**

| Trans-formation Period	GB Number	Matrix	Misorientation across GB	GB Plane
723 K, 0.4 ks	1	γ_1	[−0.990 −0.087 0.016]/25.1 deg	(0.194 −0.890 0.393)
		γ_2		(−0.109 0.880 −0.442)
	2	γ_1	[−0.290 −0.727 −0.623]/41.9 deg	(0.260 0.421 −0.863)
		γ_2		(−0.715 0.421 −0.563)
	3	γ_1	[0.232 0.674 −0.702]/61.3 deg	(0.686 0.020 0.728)
	4	γ_1	[−0.669 −0.637 0.383]/27.0 deg	(0.409 0.773 −0.513)
	5	γ_1	[0.312 −0.760 0.571]/50.3 deg	(−0.829 0.181 −0.578)
		γ_2		(0.848 −0.045 0.545)
	6	γ_1	[−0.799 −0.359 0.483]/13.0 deg	(0.635 −0.596 0.501)
	7	γ_1	[0.620 −0.435 −0.653]/52.7 deg	(0.5062 −0.517 0.696)
	8	γ_1	[0.755 −0.584 0.298]/19.8 deg	(0.008 0.483 −0.875)
		γ_2		(0.677 0.228 0.695)
	9	γ_1	[0.450 −0.510 0.733]/45.9 deg	(−0.878 0.470 −0.115)
		γ_2		(−0.504 −0.066 −0.867)
723 K, 0.7 ks	1	γ_1	[0.695 −0.057 −0.716]/45.8(deg	(−0.317 0.942 0.110)
	2	γ_1	[0.620 −0.640 0.455]/56.8 deg	(−0.271 0.923 0.273)
	3	γ_1	[−0.129 0.865 0.486]/10.6 deg	(−0.954 −0.277 −0.089)
		γ_2		(−0.189 −0.949 −0.247)
	4	γ_1	[0.124 0.615 −0.779]/48.3 deg	(0.173 −0.950 0.264)
	5	γ_1	[−0.014 −0.667 −0.779]/50.3 deg	(−0.182 −0.750 0.631)
	6	γ_1	[0.746 −0.346 0.570]/45.6 deg	(0.894 0.149 0.433)
		γ_2		(−0.065 0.750 −0.658)
	7	γ_1	[−0.969 −0.239 0.056]/41.8 deg	(−0.681 −0.466 −0.569)
		γ_2		(0.606 0.800 0.004)
	8	γ_1	[−0.564 −0.582 0.586]/59.2 deg	(−0.596 −0.617 0.516)
		γ_2		(−0.631 0.555 −0.548)
	9	γ_1	[0.495 0.544 −0.676]/43.5 deg	(0.309 0.308 0.900)
		γ_2		(−0.544 0.787 −0.296)
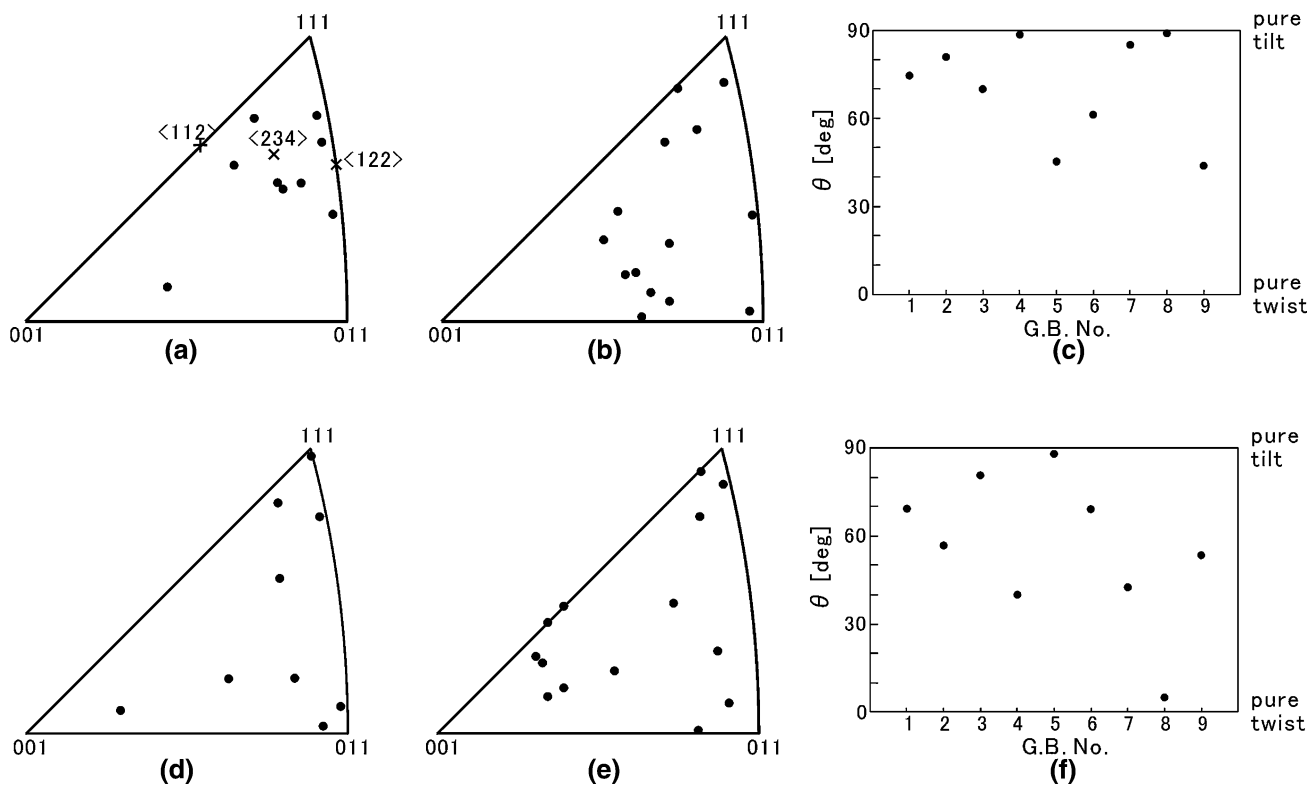
Fig. 4—Distribution of rotation axes, grain boundary plane normal, and characters of γ grain boundaries, where BFs nucleate in Fe-9Ni-0.15C at 723 K, respectively: (a) through (c) transformed for 0.4 ks and (d) through (f) transformed for 0.7 ks.
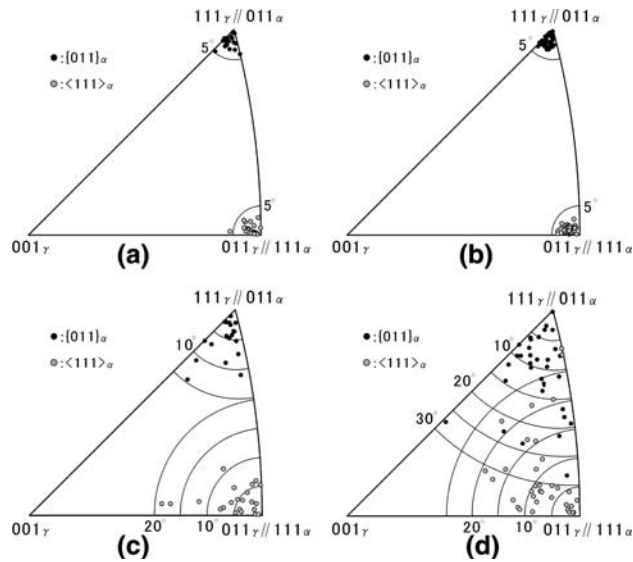
Fig. 5—Distribution of close-packed planes and close-packed directions of BF nucleated at γ grain boundaries in Fe-9Ni-0.15C at 723 K, respectively: (a) the near K-S side and (b) the near K-S side and (c) the non-K-S side, transformed for 0.4 ks and (d) the non-K-S side, transformed for 0.7 ks.

can provide the crystallographic information of BF accurately enough for the purpose of the present study.

The determination of a γ grain boundary plane was made by analyzing surface traces of the boundary in serial sectioning. Figure 1(c) schematically describes the procedure. On a polished surface containing the γ grain boundary with BFs (on the left-hand side figure), an orientation measurement was made. On this area, Vickers hardness indents were marked as positions of reference after sectioning. Then, the specimen was again polished by more than 5 μm. Since a face angle of the Vickers indenter is 136 deg, the exact depth reached by the second polishing can be estimated from a change in the size of the indent as follows:

$$\Delta z = \frac{(d/2\sqrt{2}) - (d'/2\sqrt{2})}{\tan(136 \deg/2)} = 0.1428(d - d')$$

where Δz is the depth polished, and d and d' are the diagonal lengths of the indents before and after the second polishing. The grain boundary trace also shifts by the second polishing. By measuring those horizontal shifts, Δx and Δy along the two orthogonal axes X and Y on the specimen surface and the vertical shift Δz normal to the surface along the Z axis, respectively, a normal vector to the grain boundary plane is given by the following:

$$\mathbf{n} = a \left[\frac{1}{\Delta x} \quad \frac{1}{\Delta y} \quad \frac{1}{\Delta z} \right]$$

where a is a normalizing factor. With the vector $\mathbf{n}$ and the orientations of the γ grains, the boundary plane can be indexed with respect to the γ matrices. When several measurements were made for coherent annealing twin boundaries of an austenitic stainless steel, deviations of the measured coherent twin boundary plane from $\{111\}_\gamma$

are mostly within 5 deg. The measurement of a grain boundary trace and orientations of γ grains was made on the surface after the second polishing.

B. Variant Selection Proposed for Grain Boundary Nucleation

Schematic illustrations of Figure 2 describe various selection rules of BF variants at a γ grain boundary. A BF holds the K-S OR with respect to the γ grain (γ_a) into which it grows. The rules of 1 through 3 are due to reduction of boundary energies in the BF nucleation. In rule 1 (Figure 2(a)), a BF chooses a variant that also holds a near K-S OR with respect to the opposite γ grain (γ_b), which leads to low interphase boundary energies with respect to both of the γ grains. In rule 2 (Figure 2(b)), the low energy plane (here, the parallel close-packed planes, $(111)_\gamma//(011)_\alpha$) becomes parallel to the grain boundary as much as possible. By choosing such a variant, the fraction of grain boundary area eliminated by the BF nucleation is maximized, as proposed by Lee and Aaronson.[16,17] This variant selection was previously found in fcc γ precipitation in the bcc α matrix of an (α + γ) duplex stainless steel.[18] Figure 2(c) shows a modified version for the lath- or needle-shaped phase, in which the growth direction of lath, *i.e.*, the parallel close-packed directions $[\bar{1}01]_\gamma//[\bar{1}\bar{1}1]_\alpha$, is nearly parallel to the grain boundary plane, resulting in the most effective elimination of the grain boundary area by nucleation. This kind of variant selection was previously reported in hcp α precipitation in a bcc β titanium alloy.[19]

Additionally, we propose new kinds of variant selection in terms of strain accommodation associated with BF nucleation. In Figure 2(d), a large transformation strain arises and needs to be accommodated plastically when BF nucleates coherently in γ. Here, the maximum component of strain, ε_{max}, was chosen for convenience and its relationship to the slip direction $\mathbf{b}$ in the opposite grain γ_b, or the grain boundary plane was examined since plastic accommodation can occur by the slip in the γ_b grain or by grain boundary sliding. The maximum misfit strain without plastic accommodation was calculated by following the procedure proposed by Luo and Weatherly in a fcc → bcc transformation.[20] It is considered that the variant for which ε_{max} is nearly parallel to the slip direction in the opposite γ grain or to the grain boundary plane is preferably formed. Furthermore, a similar analysis was made for a case that a lattice invariant shear deformation (LID) occurs in BF as in martensite. The LID mode of BF for the strain calculation was set by the double shear model proposed by Kelly,[21] as adopted in the previous study on the crystallography of lath martensite.[5]

III. RESULTS AND DISCUSSION

A. Overall Feature in Crystallography of Bainitic Ferrite Nucleated at Austenite Grain Boundary

Figure 3(a) shows optical microstructure of the specimen partially transformed to bainite by isothermal
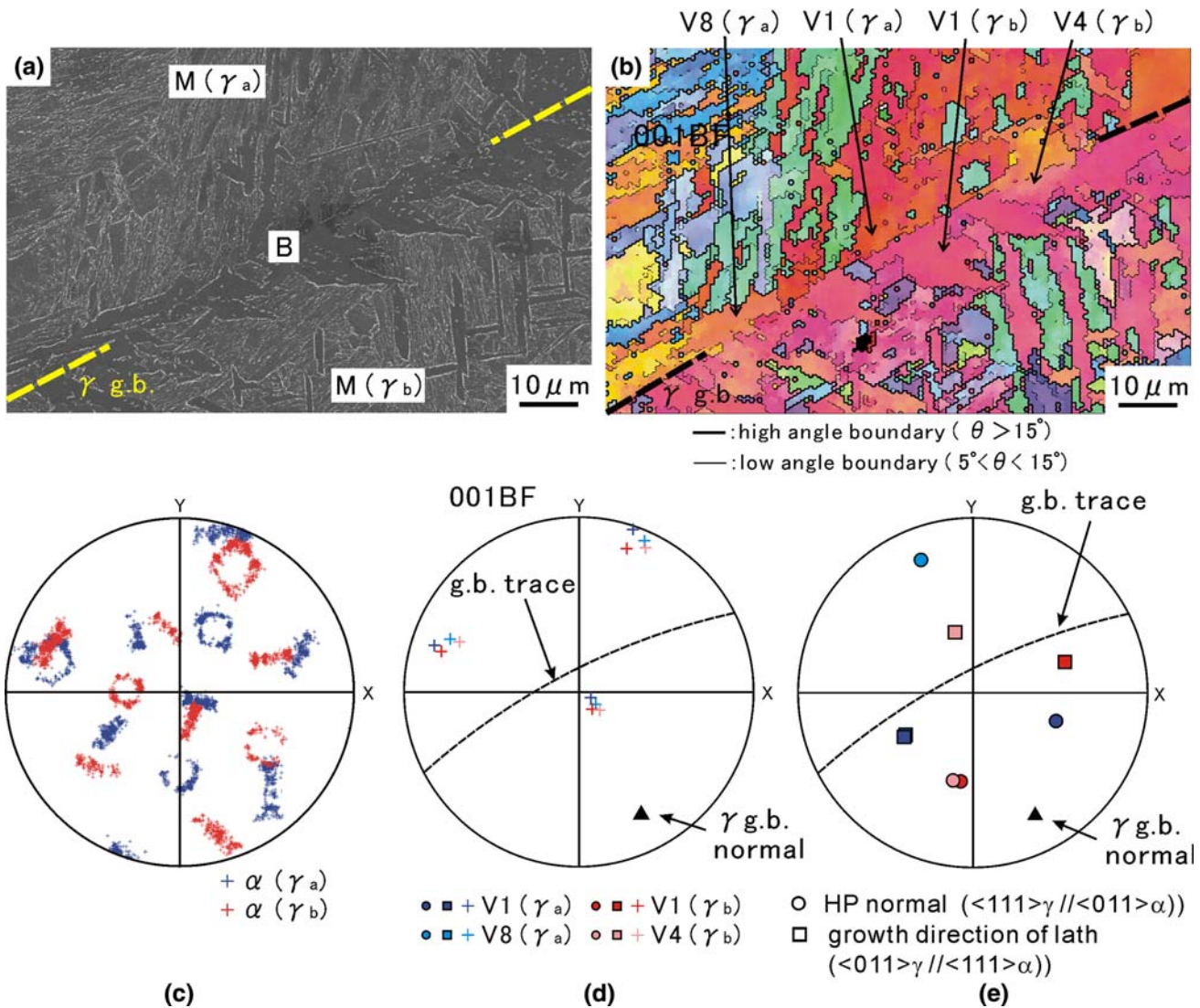
Fig. 6—(a) SEM; (b) corresponding orientation map; (c) $\langle 001 \rangle_{bcc}$ pole figure of BFs and martensites (M) formed; (d) relationship between $\langle 001 \rangle$ poles of BFs and the boundary normal, and (e) relationship between HP normal $\left(\langle 111 \rangle_{\gamma} // \langle 011 \rangle_{\alpha} \right)$, growth directions $\left(\langle 011 \rangle_{\gamma} // \langle 111 \rangle_{\alpha} \right)$ of BFs, and the boundary normal in Fe-9Ni-0.15C alloy transformed at 723 K for 0.4 ks.

holding at 723 K for 0.4 ks. Lath-shaped BF (denoted as *B*) nucleates at some γ grain boundaries, and each of them grow into one γ grain, forming the boundary. In Figure 3(b), showing the microstructure of the specimen transformed for 0.7 ks, some γ grain boundaries are still free from BFs, as pointed out by white arrows, whereas others are fully covered with BFs (black arrows). This observation implies that the potency as a BF nucleation site is different for each boundary.

Table II shows the characteristics of γ austenite grain boundaries where BF nucleates at 723 K. The grain boundaries with BFs are mostly high-angle boundaries. Figure 4 represents rotation axes, boundary planes, and angles between the rotation axis and the boundary plane of the γ grain boundaries listed in Table II. In the standard stereographic triangle of Figure 4(a), the rotation axes scatter around $\langle 234 \rangle_{\gamma}$ in the early stage of bainite transformation, although they distribute more

randomly as the transformation proceeds in Figure 4(d). The boundary planes do not show apparent localization (Figures 4(b) and (e)). Figures 4(c) and (f) indicate that tilt boundaries are selected more preferentially than twist ones as the nucleation site of BF.

Stereographic triangles in Figure 5 show angular deviation between close-packed planes as well as close-packed directions in BFs and its γ matrices. The BFs hold near K-S relationships with respect to one of the adjacent γ grains (Figures 5(a) and (c)), with deviations less than 5 deg. With respect to the opposite γ grain, the orientation relationships of BF are also close to the K-S relationship within deviations less than 10 deg in the specimen transformed for 0.4 ks (Figure 5(b)). However, in the specimen transformed for 0.7 ks, the deviation becomes much larger than the early stage of bainite transformation and the maximum deviation detected reached up to 30 deg (Figure 5(d)).
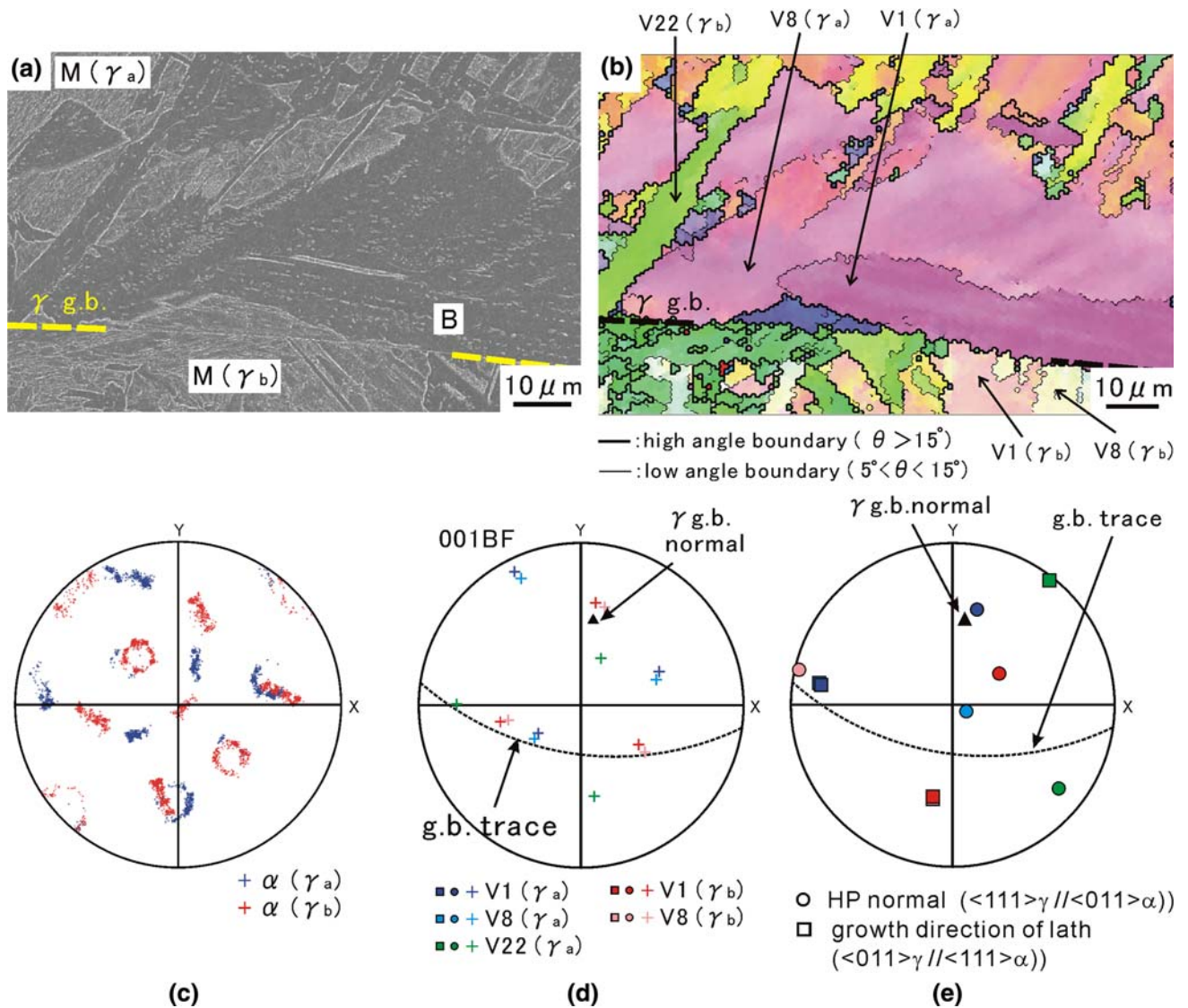
Fig. 7—(a) SEM; (b) corresponding orientation map; (c) ⟨001⟩ bcc pole figure of BFs and martensites (M) formed; (d) relationship between ⟨001⟩ poles of BFs and the boundary normal; and (e) relationship between HP normal $\left(\langle 111\rangle_\gamma // \langle 011\rangle_\alpha\right)$ growth directions $\left(\langle 011\rangle_\gamma // \langle 111\rangle_\alpha\right)$ of BFs, and the boundary normal in the Fe-9Ni-0.15C alloy transformed at 723 K for 0.7 ks.

B. Characteristic of Variant for Bainitic Ferrite in Grain Boundary Nucleation

Figure 6(a) is a scanning electron micrograph of BF laths nucleated at a γ grain boundary in the specimen transformed at 723 K for 0.4 ks. The BFs nucleate at both sides of the grain boundary. Figures 6(b) through (e) describe the BF crystallography determined by EBSD and serial sectioning analyses. Figure 6(c), the ⟨001⟩ bcc pole figure of BFs and LMs in the area of Figure 6(b), shows that the misorientations between BF and LM blocks are well explained as intervariant relationships of the K-S orientation relationship, as already mentioned in Figure 1. The orientation map in Figure 6(b) shows that specific BF variants, V1, V4, and V8, are formed at this boundary. As was reported previously,[2] an upper bainite packet often consists of the BF laths of only two variants with a small misorientation (approximately

10 deg) at 723 K. Both V1 and V4 correspond to this specific combination of BF variants. V8 is also misoriented with V1 by about 10 deg, but they belong to different packets, as shown in Table I. Formation of this variant combination was reported by Lambert-Perlade et al.[13] It is also noted that the two BF blocks, each of which grows into a different γ grain, are misoriented by small angles, implying that deviation from the K-S orientation relationship in the opposite γ grain is small for those BFs.

Figures 6(d) and (e) show the relationships between the boundary normal and ⟨001⟩ poles of BFs and HP normal $\left(\langle 111\rangle_\gamma // \langle 011\rangle_\alpha\right)$ as well as the growth directions $\left(\langle 011\rangle_\gamma // \langle 111\rangle_\alpha\right)$ of BFs. In Figure 6(e), the HP normal, i.e., $\langle 111\rangle_\gamma // \langle 011\rangle_\alpha$, is far from the grain boundary normal. This indicates that the low energy interface of

Table III. Various Relationships of BF Variant and γ Grain Boundary Characteristics in Fe-9Ni-0.15C Alloy Transformed at 723 K for 0.4 ks

GB Number	Matrix Grain	BF Variant Number	Misorientation from K-S in the Opposite Grain γ_b (Deg)	Angle between HP and GB (Deg)	Angle between Growth Direction and GB (Deg)	Angle between ε_{max} and GB (Deg)		Angle between ε_{max} and Slip Direction (**b**) in the Grain γ_b (Deg)	
						No LID	With LID	No LID	With LID
1	γ_1	V1	5.1	80.6	8.2	12.8	18.5	26.4	1.7
		V5	19.0	80.6	51.1	20.1	14.4	30.8	24.6
	γ_2	V1	5.1	79.7	13.9	11.9	17.0	25.9	3.6
2	γ_1	V1	5.2	84.1	53.1	20.6	13.8	28.6	17.7
	γ_2	V1	5.2	59.7	5.9	51.8	14.5	24.5	30.1
3	γ_1	V1	8.2	33.9	1.7	78.5	41.0	17.9	17.3
		V8	12.3	36.7	1.7	44.1	74.1	28.1	24.4
4	γ_1	V1	6.3	68.0	39.1	4.0	15.8	21.8	19.5
5	γ_1	V1	7.4	49.6	10.8	60.0	21.8	39.0	13.7
		V8	4.7	24.5	10.8	47.8	82.0	27.6	16.1
	γ_2	V1	6.4	39.6	12.5	66.9	30.0	29.8	21.4
		V4	4.7	39.6	23.5	63.7	28.4	26.2	18.1
6	γ_1	V1	5.6	72.4	5.9	38.7	2.1	8.0	16.1
7	γ_1	V1	6.9	66.6	7.9	45.6	12.5	18.1	36.6
8	γ_1	V1	2.9	77.0	38.5	31.3	14.6	14.9	17.0
	γ_2	V1	2.9	22.1	0.7	90.0	50.3	18.1	13.0
9	γ_1	V1	4.5	72.7	32.9	32.8	4.6	25.2	15.4
	γ_2	V1	4.6	34.6	14.9	73.7	47.0	30.5	23.2
		V8	10.6	41.6	14.9	47.4	63.5	15.7	42.6

BF is inclined to the grain boundary by large angles. This is quite different from the variant selection rule described in Figure 2(a). In Figure 6(e), the parallel close-packed direction for the BF variant, which is the growth direction of BF lath, is also close to being parallel to the grain boundary plane. This corresponds to the rule described in Figure 2(b).

Figure 7 shows a typical result of the EBSD/serial sectioning analysis made in the specimen transformed at 723 K for 0.7 ks, which is in the late stage of transformation. The scanning electron micrograph (Figure 7(a)) and the corresponding orientation map (Figure 7(b)) of BF laths nucleated at the γ grain boundary have revealed that the specific combination of BF variants, V1 and V8, misoriented by a small angle is again observed in each γ grain. Also, at this stage, other BF variants, V22 in this figure, begin to nucleate. Figures 7(b) through (e) describe the BF crystallography determined by EBSD and serial sectioning analyses. In this case, the BF blocks, each of which grows into a different γ grain, are misoriented by a large angle. Figures 7(d) and (e) show the relationship between the boundary normal and $\langle 001 \rangle$ poles of BFs and HP normal $\left(\langle 111 \rangle_\gamma // \langle 011 \rangle_\alpha \right)$ as well as growth directions $\left(\langle 011 \rangle_\gamma // \langle 111 \rangle_\alpha \right)$ of BFs. In Figure 7(e), the parallel close-packed direction for the BF variant is also close to being parallel to the grain boundary plane, except V22.

In the present study, 19 BF variants at nine γ grain boundaries in the specimen transformed for 0.4 ks and 34 BF variants at nine γ grain boundaries in the specimen transformed for 0.7 ks were analyzed,

respectively. Tables III and IV represent the comparison between the BF variants experimentally determined and the selection rules described in Figure 2 for the BFs observed in those two specimens, respectively. Table V summarizes the preference in variant selection of BF for grain boundary nucleation. Here, the misorientation allowed in judging satisfaction of the variant selection rule is taken as 10 deg in rule 1 and 15 deg for the other rules.

In the specimen transformed for 0.4 ks, many γ boundaries accompany a single BF variant on each side of the boundary (defined as V1 in Table I). It is seen that most of the BFs have misorientation from the K-S orientation relationship smaller than 10 deg with respect to the opposite γ grain, indicating that the variant selection rule 1 in Figure 2(a) is dominant. Also, a fraction of rule 3 in which the growth direction of BF lath is close to parallel to the γ grain boundary plane is large. It is surprising that the habit plane of BF does not play a significant role in the variant selection (see the small contribution of rule 2). This can be attributed to the lath-shaped morphology of BF presumably because the K-S orientation relationship only provides a single invariant line with no misfit and no rotation with a small rigid body rotation.[20] When the BF lath lies along the boundary plane, the grain boundary area can be eliminated effectively by nucleation, leading to the predominant contribution of rule 3.

There are many γ grain boundaries without BFs after the BF nucleation under the abovementioned strong variant selection. Thus, as transformation proceeds, different variant selection rules become more active. As a result, the fractions of the selection rules 1 and 3 both

Table IV. Various Relationships of BF Variant and γ Grain Boundary Characteristics in Fe-9Ni-0.15C Alloy Transformed at 723 K for 0.7 ks

GB Number	Matrix Grain	BF Variant Number	Misorientation from K-S in the Opposite Grain γ_b (Deg)	Angle between HP and GB (Deg)	Angle between Growth Direction and GB (Deg)	Angle between ε_{max} and GB (Deg)		Angle between ε_{max} and slip direction (**b**) in the grain γ_b (Deg)	
						No LID	With LID	No LID	With LID
1	γ_1	V1	4.5	65.0	17.5	5.0	42.4	29.6	30.4
		V8	14.3	48.4	17.5	34.1	21.7	19.6	29.7
2	γ_1	V1	8.9	58.2	22.6	12.9	51.0	21.9	30.9
		V20	9.5	77.2	57.7	8.3	28.0	23.8	27.8
3	γ_1	V1	8.1	40.0	37.7	49.2	27.2	14.6	8.9
		V5	8.1	40.0	28.4	64.0	50.4	22.0	12.3
	γ_2	V1	3.2	58.8	18.3	9.6	32.8	5.4	16.5
		V20	8.1	36.7	32.3	32.1	63.0	18.7	4.5
		V22	4.7	36.7	20.7	64.5	55.2	6.7	16.8
4	γ_1	V1	17.1	72.7	2.9	4.7	27.6	13.4	29.9
5	γ_1	V1	15.4	80.3	35.1	9.9	7.9	18.1	9.0
		V6	19.2	80.3	24.3	13.7	27.9	13.5	31.8
6	γ_1	V1	9.1	32.0	19.2	66.9	34.9	16.9	37.9
		V4	8.5	32.0	10.9	63.1	34.3	20.9	38.8
		V13	3.8	79.5	10.9	11.4	18.2	26.6	18.5
	γ_2	V1	19.0	39.3	31.0	37.0	74.2	34.6	5.8
		V4	21.3	39.3	3.8	40.0	73.8	32.6	6.2
		V8	9.6	84.6	31.0	1.9	11.5	22.2	31.5
7	γ_1	V1	36.8	8.8	4.4	74.0	57.8	18.5	24.2
		V8	28.1	62.9	4.4	19.2	50.6	28.6	15.7
		V22	21.3	70.9	46.7	38.0	0.3	13.0	34.4
	γ_2	V1	29.1	35.8	24.7	35.6	43.6	39.2	18.4
		V3	25.1	83.8	24.7	18.9	16.9	28.9	24.4
		V8	23.2	35.8	34.0	45.9	74.9	16.1	23.7
8	γ_1	V1	20.9	66.5	51.7	9.0	11.7	14.4	11.3
		V5	10.3	66.5	0.8	45.1	9.2	38.8	12.4
		V15	11.3	73.4	3.0	38.6	4.2	38.9	10.6
		V18	15.3	73.4	58.9	37.9	0.8	36.7	12.4
	γ_2	V1	10.0	68.8	3.4	42.8	6.4	38.4	11.5
		V24	14.5	74.5	56.1	36.2	1.2	37.3	14.5
9	γ_1	V1	8.1	28.8	24.6	67.6	62.4	25.8	13.3
		V5	24.5	28.8	0.6	39.2	65.6	29.5	26.6
		V19	19.5	80.5	0.6	12.4	21.7	10.0	29.6
	γ_2	V1	12.3	88.5	10.4	22.4	14.6	13.0	34.5

Table V. Changes in the Behavior of Variant Selection of BF at γ Grain Boundary with Transformation Period (N_{GB}: Number of γ Grain Boundaries Observed, and N_{total}: Number of BF Variants Observed)

Transformation Period at 723 K	Rule 1 Small Misorientation from K-S in γ_b	Rule 2 HP ~//GB	Rule 3 Growth Direction ~//GB	Rule 4 ε_{max} (No LID) ~//GB	Rule 5 ε_{max} (With LID) ~//GB	Rule 6 ε_{max} (no LID) ~//**b** in γ_b	Rule 7 ε_{max} (with LID) ~//**b** in γ_b
0.4 ks (N_{GB} = 9, N_{total} = 19)	84 pct	0 pct	68 pct	16 pct	37 pct	11 pct	21 pct
0.7 ks (N_{GB} = 9, N_{total} = 34)	38 pct	3 pct	35 pct	33 pct	29 pct	26 pct	38 pct

decrease, and, instead, rules 4 through 7, which are advantageous in strain accommodation, become important. However, it is not clear whether accommodation along the grain boundary (rules 4 and 5) or in the opposite grain (rules 6 and 7) is more important. A question, which of elastic strain or strain after plastic accommodation (in other words, which of the rules 4 and 6 or the rules 5 and 7) affects the variant selection, also remains.

C. *Effect of Crystallography on Bainite Block Size*

The present analysis has shown clearly that there is strong variant selection of BF by γ matrix grain

boundaries in the upper bainite structure. The block size of upper bainite should be affected significantly by the natures of their nucleation sites, since variant selection often results in the formation of preferred variants on such sites. As previously reported,[2] BFs formed at 723 K exhibit a coarse size of blocks due to such variant selection.

As this selection is weaker, more BF variants form at a γ matrix grain boundary, and thus, the bainite block width becomes finer. The factors that weaken the variant selection are the driving force for the transformation and self-accommodation of transformation strain. For a larger driving force, which can be achieved by lowering the carbon content or transformation temperature, the difference in the activation energy for nucleation between BF variants should be smaller and more variants are able to nucleate. Self-accommodation of transformation strain by formation of different variants in neighbors should be enhanced when plastic accommodation in γ and also in BF is difficult. Such a situation is achieved, for example, by strengthening of austenite through lowering transformation temperature or increasing carbon content. Indeed, a BF packet starts to contain BF blocks of all six variants possible as the temperature is lowered.[2] Although similar variant selection was still recognized in the early transformation stage even at 673 K, it is considered that self-accommodation is mainly responsible for the formation of different BF variants in a packet.

IV. CONCLUSIONS

The crystallography of bainitic ferrite nucleated at austenite grain boundaries was studied in an Fe-9Ni-0.15C alloy. The relationship between variants of bainitic ferrite and grain boundary characters, *i.e.*, misorientation and a boundary orientation, was examined by combining electron backscatter diffraction measurement in scanning electron microscopy and serial-sectioning polishing. Bainitic ferrite nearly holds the K-S orientation relationship with respect to the austenite grain into which it grows. Deviation of the orientation relationship with respect to the opposite austenite grain from the K-S one is relatively small, and low-angle boundaries are often formed between the bainitic ferrites adjacent to each other across the prior austenite grain boundary. Also, the parallel close-packed direction of the K-S variant, which corresponds to the longitudinal direction of bainitic ferrite lath, is nearly parallel to the grain boundary plane. As transformation proceeds, secondary variant selection preferred in terms of plastic accommodation of transformation strain becomes more active. Such variant selection of bainitic ferrite leads to the coarsening of bainite block size at a small undercooling reported recently.[2]

ACKNOWLEDGMENTS

APPENDIX

Calculation of transformation strain

Transformation strain without or with plastic accommodation was estimated by the phenomenological theory of martensite crystallography.

During fcc → bcc martensitic transformations, the Bain lattice correspondence is maintained accommodation. Under this correspondence, the following Bain strain is generated:

$$\mathbf{B} = \begin{pmatrix} \sqrt{2}\,a_\alpha/a_\gamma & 0 & 0 \\ 0 & \sqrt{2}\,a_\alpha/a_\gamma & 0 \\ 0 & 0 & a_\alpha/a_\gamma \end{pmatrix}$$

Here, three orthogonal axes are set to be $[100]_\gamma//[110]_\alpha$, $[010]_\gamma//[\bar{1}10]_\alpha$, and $[001]_\gamma//[001]_\alpha$. Assuming the K-S orientation relationship between BF and the γ matrix, $(111)_\gamma//(011)_\alpha$, $[\bar{1}01]_\gamma//[\bar{1}\bar{1}1]_\alpha$, the transformation strain can be given by the Bain strain and the rigid body rotation;

$$\mathbf{F} = \mathbf{T_2} \cdot \mathbf{T_1} \cdot \mathbf{B}$$

In the preceding equation, $\mathbf{T_1}$ and $\mathbf{T_2}$ are matrices that accomplish clockwise rotations of 9.74 deg around $[1\bar{1}0]_\gamma$ and of 5.26 deg around $[111]_\gamma$, respectively. To calculate the maximum misfit strain, the method previously used by Luo and Weatherly[20] was applied. The misfit strain along a given direction $\mathbf{p} = [x, y, z]$ is described as follows:

$$\mathbf{b} = ((\mathbf{T_2} \cdot \mathbf{T_1} \cdot \mathbf{B})^{-1} - \mathbf{I}) \cdot \mathbf{p}$$

The maximum strain of a magnitude of 0.3878 is obtained along $\mathbf{p_{max}} = [0.6534, 0.2312, 0.7208]_\gamma$ by solving the following conditions:

$$\frac{\partial |\mathbf{b}|}{\partial x} = \frac{\partial |\mathbf{b}|}{\partial y} = 0, \; z^2 = 1 - x^2 - y^2$$

To estimate the strain after accommodation, a double shear LID model proposed by Kelly[21] to analyze the crystallography of LM was applied as in the previous study.[9]

$$\mathbf{F'} = \mathbf{R} \cdot \mathbf{B} \cdot \mathbf{S_2} \cdot \mathbf{S_1}$$

where $\mathbf{R}$ is the rigid body rotation, and $\mathbf{S_1}$ and $\mathbf{S_2}$ are the matrices that represent lattice invariant shear for $(hhl)[1\bar{1}0]_\gamma$ and $(hll)[0\bar{1}1]_\gamma$ slip modes, respectively. The direction of the maximum strain is $\mathbf{f_{max}} = [-0.2013, -0.7071, -0.6779]_\gamma$. Then, the misorientations of those directions and the grain boundary plane or slip directions in the opposite matrix grain γ_2 were analyzed in each BF.

REFERENCES

1. Y. Ohmori, H. Ohtani, and T. Kunitake: *Trans. ISIJ*, 1971, vol. 11, pp. 250–59.
2. T. Furuhara, H. Kawata, S. Morito, and T. Maki: *Mater. Sci. Eng. A*, 2006, vol. 431, pp. 228–36.
3. T.E. Swarr and G. Krauss: *Metall. Trans. A*, 1976, vol. 7A, pp. 41–48.
4. M.J. Roberts: *Metall. Trans.*, 1970, vol. 1, pp. 3287–94.
5. S. Morito, H. Yoshida, T. Maki, and X. Huang: *Mater. Sci. Eng. A*, 2006, vol. 438, pp. 237–40.
6. S. Matsuda, T. Inoue, and M. Ogasawara: *Trans. JIM*, 1968, vol. 9, pp. 343–48.
7. S. Matsuda, T. Inoue, H. Mimura, and Y. Okamura: *Trans. ISIJ*, 1972, vol. 12, pp. 325–33.
8. A.F. Gourgues, H.M. Flower, and T.C. Lindley: *Mater. Sci. Technol.*, 2000, vol. 16, pp. 26–40.
9. S. Morito, H. Tanaka, R. Konishi, T. Furuhara, and T. Maki: *Acta Mater.*, 2003, vol. 51, pp. 1789–99.
10. H. Kitahara, R. Ueji, N. Tsuji, and Y. Minamino: *Acta Mater.*, 2006, vol. 54, pp. 1279–88.
11. T. Maki, K. Tsuzaki, and I. Tamura: *Trans. ISIJ*, 1980, vol. 20, pp. 207–14.
12. E. Bouyne, H.M. Flower, T.C. Lindley, and A. Pineau: *Scripta Mater.*, 1998, vol. 39, pp. 295–300.
13. A. Lambert-Perlade, A.F. Gourgues, and A. Pineau: *Acta Mater.*, 2004, vol. 52, pp. 2337–48.
14. H. Kawata, K. Sakamoto, T. Moritani, T. Furuhara, S. Morito, and T. Maki: *Mater. Sci. Eng. A*, 2006, vol. 438, pp. 140–44.
15. T. Furuhara and T. Maki: *Mater. Sci. Eng. A*, 2001, vol. 312, pp. 145–54.
16. J.K. Lee and H.I. Aaronson: *Acta Metall.*, 1979, vol. 23, pp. 799–808.
17. J.K. Lee and H.I. Aaronson: *Acta Metall.*, 1979, vol. 23, pp. 809–20.
18. K. Ameyama, T. Maki, and I. Tamura: *J. Jpn. Inst. Met.*, 1986, vol. 50, pp. 602–11.
19. T. Furuhara, S. Takagi, H. Watanabe, and T. Maki: *Metall. Mater. Trans. A*, 1996, vol. 27A, pp. 1630–41.
20. C.P. Luo and G.C. Weatherly: *Acta Metall.*, 1987, vol. 35, pp. 1963–72.
21. P.M. Kelly: *Mater. Trans. JIM*, 1992, vol. 33, pp. 235–42.